ARTICLES

Zeolitic Inorganic−Organic Polymer Electrolyte Based on Oligo(ethylene glycol) 600 K_2PdCl_4 and $K_3Co(CN)_6$

Vito Di Noto†

Dipartimento di Chimica Inorganica, Metallorganica ed Analitica, Università di Padova, via Loredan 4, I-35135 Padova, Italy

Received: September 14, 1999; In Final Form: January 28, 2000

Acqueous solutions of K_2PdCl_4 and $K_3Co(CN)_6$ were combined separately with PEG600 and then reacted together, giving rise to a sol → gel transition followed by a gel → plastic transition. This reaction scheme produced a new zeolitic inorganic−organic polymer electrolyte, $[Co_xPd_y(CN)_zCl_v(CH_{2n}H_{4n+2}O_{n+1})K_l]$. Rheological investigations carried out by a dynamic oscillatory method demonstrated that the sol → gel transition is strongly affected by temperature. Indeed, the gelation process produced the most robust solid gel structure in the shortest time when conducted at elevated temperatures. TG measurements demonstrated that the synthesized polymer electrolyte is thermally stable up to ca. 210 °C. Scanning electronic microscopy showed that the material consists of a compact granular paste. On the basis of mid and far Fourier transform infrared spectroscopy and analytical data, it was concluded that the synthesized material is a zeolitic inorganic−organic network where CN bridges bond together Co and Pd atoms and PEG600 bridges Pd atoms. Conductivity of the product was investigated by impedance spectroscopy in the temperature and frequency ranges of 20−80 °C and 20 Hz to 1 MHz, respectively; results demostrated that the polymer electrolyte conducts ionically by two distinct conductivity regions which follow Arrhenius type equations. At 25 °C the conductivity of the material is on the order of 3×10^{-5} S cm^{-1}. A mechanism based on the jump relaxation model is proposed to explain the conductivity of the polymer.

Introduction

At present, academic and industrial researchers are devoting particular attention to the development of electroactive polymers.[1,2] These systems are usually classified in two groups, i.e., polymer materials exhibiting ionic conductivity and those with an electronic transport mechanism.[3] The ionically conducting materials, which are commonly termed "polymer electrolytes", are of great importance for the fabrication of portable battery-operated electric equipment such as computers, tools, video cameras, etc. and for the development of battery-powered electric vehicles.

Further significant advances in the technical application of electrochemical energy storage systems may depend almost completely on the rate at which useful new polymer electrolytes can be devised and synthesized.

The most extensively studied polymer electrolyte systems have been obtained by doping poly(ethylene oxide) (PEO), poly(ethylene glycol) (PEG), poly(propylene glycol) (PPG) or poly(propylene oxide) (PPO) with one or a mixture of inorganic salts such as $LiClO_4$, $LiCF_3SO_3$, LiSCN, NaSCN, KSCN, etc.[4−8] This group of polymer electrolytes are referred to as polymer electrolytes of the first category,[1] or "class 1". The relatively low ionic conductivity of these materials has prompted the development of four additional classes.[1] Class 2 materials are gel electrolytes formed by dissolving a solution of a salt in a polar liquid in an inactive polymeric material having good mechanical stability.[1,9] Class 3 are the so-called "plasticized electrolytes", prepared by combining a conducting polymer electrolyte with a small quantity of a solvent with a high dielectric constant.[3] Class 4 materials are commonly referred to as the "ionic rubbers", which are obtained by addition of a small amount of a high molecular weight polymer to a liquid electrolyte.[1] Class 5 materials ("membrane ionomers") are proton conducting polymer electrolytes that are receiving special attention for their application in fuel cell technology.

In an attempt to increase the conductivity of these materials, it was recently proposed that classical polymer electrolytes could be modified by introducing inorganic oxides into their matrix.[10−12] In these materials, the dissolved oxide particles create grain boundaries which are responsible for the formation of highly conductive layers at the polymer-ceramic interfaces and prevent the polymeric chains from crystallizing.[13,14] Indeed, it was claimed that these (nano)composite polymer electrolytes (CPE) exhibit an amorphous behavior which is guaranteed by the inorganic component, and they appear to be good candidates for use in lithium batteries.

Up to now, the integration of half-metal or metals as heteroatoms has remained a marginal topic in polymer electrolyte chemistry. Several studies have been aimed at the insertion of silicium[15] and titanium[16] in to the backbone of poly(ethylene oxide) chains of polymer electrolytes. Innovative examples of metallorganic hybrids having transition metal atoms integrated

† E-mail: dinoto@ux1.unipd.it.

10.1021/jp9932719 CCC: $19.00 © 2000 American Chemical Society
Published on Web 10/19/2000

as heteroatoms into a poly(ethylene glycol) backbone are the so-called "zeolitic inorganic-organic polymer electrolytes" (Z-IOPE) formed by K_2PdCl_4, $K_3Fe(CN)_6$ and poly(ethylene glycol) 600 (PEG600). Considering their high conductivity at room temperature ($\cong 1.4 \times 10^{-3}$ S cm^{-1}), these materials appear to be very promising for technical applications.[17]

In this paper we describe the synthesis and characterization of $[Co_xPd_y(CN)_zCl_t(CH_{2n}H_{4n+2}O_{n+1})K_l]$, a new Z-IOPE material based on poly(ethylene glycol) 600, K_2PdCl_4 and $K_3Co(CN)_6$. In particular, the aim of the present study was to obtain a new inorganic−organic network based on $K_3Co(CN)_6$, K_2PdCl_4 and PEG600 via sol → gel, gel → plastic transitions. The transitions leadings to the production of the new Z-IOPE were studied by rheological measurements. The conformation of the polyether chain in the Z-IOPE material was determined by FT-IR spectroscopy, its conductivity was measured at different temperatures, and its morphology was examined by electron microscopy.

Experimental Section

Reagents. K_2PdCl_4 and $K_3Co(CN)_6$ (Aldrich ACS reagents) were used as supplied. PEG of molecular weight 600 (Aldrich ACS reagents) was further purified by standard methods and stored under argon on 4A activated molecular sieves to prevent contamination by moisture. In addition, all transfer and handling operations were performed in an argon atmosphere.

Instrumentation and Methods. The FT-IR spectra in mid-infrared (MIR) and far-infrared (FIR) were recorded by using a Nicolet 5SxC spectrophotometer equipped with a tryglycine sulfate (TGS) detector at a nominal resolution of 4 cm^{-1} and collecting 900 scans; the Happ-Genzel apodization method was adopted.[18] The sample was distributed as a thin film between two windows composed of KBr or polyethylene for MIR and far-IR measurements, respectively and transferred into a sealed cell.

The amounts of Co, Pd and K in the product were determined by inductively coupled plasma atomic emission spectrometry (ICP-AES) by using the method of standard additions and the following emission lines: λ(Co) = 228.616 nm; λ(Pd) = 340.458 nm; λ(K) = 766.490 nm. The ICP-AES measurements were carried out by using a Spectroflame Modula sequential and simultaneous spectrometer equipped with a capillary cross-flow nebulizer (Spectro Analytical, Kleve, Germany). The element determinations were performed using a plasma power of 1.2 kW, a radio frequency generator of 27.12 MHz and an argon gas flow in nebulizer, auxiliary, and coolant set at 1, 0.5, and 14 L/min, respectively. The solution suitable for ICP-AES analysis was obtained by microwave sample digestion using a CEM MDS-2100 microwave sample preparation system after treating a suitable amount of the product with a solution of 54%-(v/v) HNO_3 (70%), 31% (v/v) HCl (37%), 15% (v/v) H_2O.

Thermogravimetric (TG) analysis was performed using a Perkin-Elmer TGS-2 thermobalance, operating in a nitrogen atmosphere inside a Braun MB-150 I/II drybox. The TG profile was recorded under a working N_2 dynamic flux of 50 cm^3 min^{-1} and at a heating rate of 20 °C min^{-1}.

The morphology of the samples was examined by scanning electron microscopy (SEM) using a Cambridge Stereoscan 250 Mark 1 electron microscope at an acceleration voltage of 20 kV. The samples were coated with graphite film using a Balzer mod. Med. 010(6) unit operating at 0.2 mbar from 20 °C to 80 °C.

Elemental X-ray fluorescence microanalysis was carried out by using the SEM microscope described above equipped with an energy-dispersive X-ray spectrometer (EDX) EDAX PW9800 operating with a Si/Li detector.

ac impedance measurements were carried out in the 20 Hz to 1 MHz frequency range by using a computer-controlled HP4284A precision LCR Meter. The sample in pellet form was placed in a compartment within a homemade cell consisting of two cylindrical gold-plated stainless steel elecrodes joined by a Teflon ring. The diameter of the electrode−electrolyte contact surface and the distance between the electrodes were determined by micrometer measurements and no correction was made for the thermal expansion of the cell. The temperature was measured with an accuracy greater than ±0.1 °C.

Rheological measurements were performed by using a Haake Rheo Stress RS 100 instrument equipped with a PP35 parallel plate sensor with a gap of 0.5 mm. The time scans were determined in the 30−70 °C temperature range.

The electrochemical stability of the sample was determined by voltametric studies using a Potentiostat/Galvanostat (model 263A, EG and G Instruments). The working electrode was a small-diameter Pt wire sealed in a glass capillary (geometric surface of 1.23×10^{-4} cm^2), the counter electrode was a Pt wire (0.6 mm diameter) and the reference electrode was an Ag/AgCl wire (ca 0.4 mm diameter). The scans were taken at 100 mV/s.

Synthesis of $[Co_xPd_y(CN)_zCl_t(CH_{2n}H_{4n+2}O_{n+1})K_l]$. The new polymer electrolyte was prepared as follows. A solution of K_2PdCl_4 (brown in color) was obtained by dissolving 0.4901 g (1.50×10^{-3} mol) of K_2PdCl_4 in 2.20 g of water with heating and stirring; a separate solution of $K_3Co(CN)_6$ (colorless) was prepared by dissolving 0.2550 g (7.7×10^{-4} mol) of $K_3Co(CN)_6$ in 2.21 g of water.

PEG600 (2.18 g) was added to the Pd and Co solutions at room temperature with stirring, resulting in solutions A and B, respectively. Solutions A and B were then mixed together, resulting in a solution whose color gradually changed from brown to orange.This mixture was then left undisturbed. Within a period of 24 h an increase in viscosity was observed which then gave rise to a hard, transparent polymeric hydrogel with a glassy, yellow-orange appearance. The consistency of this solid was such that the gel network remained undisturbed upon inversion of the container.

After a few weeks, the material slowly released a transparent solvent and shrank in volume. We then broke the polymer into smaller pieces to accelerate solvent release, and after 2 days filtered and dried it at room temperature and at 10^{-6} mbar for 1 week. The resulting polymer was stored under argon atmosphere and exhibited a clear pale green color.

The percentages of Pd, Co and K in the polymer were determined by ICP-AES spectrometry and by using the method of standard additions in the range of 0−100 ppb, after microwave digestion of 115.4 mg of the sample.

Results and Discussion

Reaction Observations. Two separate solutions of K_2PdCl_4 (solution A) and $K_3Co(CN)_6$ (solution B), each prepared in a mixture of PEG600 and H_2O, were mixed together (step a) of Scheme 1), resulting in a homogeneous liquid with a transparent brown color, the weight composition of which is reported in Table 1.

This material formed a hard solid gel within 6 h when left undisturbed (step b) of Scheme 1). This sol → gel transition probably takes place owing to well-established reactions:[19,20] the Cl^- ligand, which is a good leaving ligand in $PdCl_4^{2-}$, may be substituted by either the nitrogen atom of cyanometalate (i.e.,

SCHEME 1: Synthesis of a Polymer Electrolyte System Based on Oligo(ethylene glycol) 600, K_2PdCl_4 and $K_3Co(CN)_6$

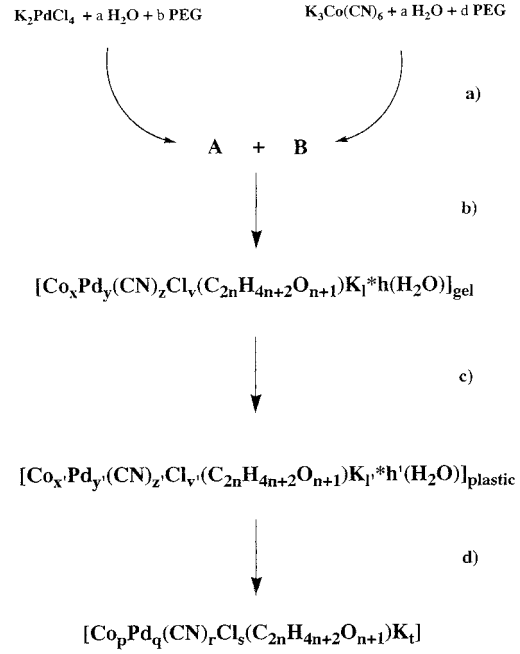

TABLE 1: Weight Composition of the Reaction Mixture for the Synthesis of Polymeric $[Co_xPd_y(CN)_zCl_v(C_{2n}H_{4n+2}O_{n+1})K_l]$

$K_3[Co(CN)_6]$/g	K_2PdCl_4/g	PEG600/g	H_2O/g
0.2550	0.4901	4.360	4.41

$[Co(CN)_6]^{3-}$) or by the hydroxyl group of water or PEG600. As reported in the literature,[21,22] the substitution of Cl^- in $[PdCl_4]^{2-}$ by nitrogen ligands is preferred because more stable complexes are obtained. In practice, we belive that this sol → gel reaction happens owing to two phenomena which take place simultaneously: (a) the direct nucleophilic displacement of Cl^- by the ligands[19] and (b) the indirect substitution of Cl^- in $[PdCl_4]^{2-}$. This latter event occurs due to the slow displacement of Cl^- by H_2O, which is then replaced by the cyanometalate or PEG600 hydroxyl ligands. In this case H_2O acts as a catalyst. This reaction mechanism is strongly supported by the observation that the use of pure PEG600 in the absence of H_2O did not lead to gel formation, and that the gel decreased in volume throughout step c) of Scheme 1, releasing a transparent liquid composed mainly of H_2O and traces of PEG600, K^+, Cl^- and Pd. It is reasonable to assume that the gel → plastic transition occurs mainly owing to the slow indirect substitution reaction previously discussed.

The final Z-IOPE product, which is obtained after step d) of Scheme 1, is very stable and presents the consistency of a smooth solid plastic paste. In this reaction step the material is treated and dried in order to eliminate all traces of water and other components and stored under argon atmosphere.

Table 2 summarizes the analytical data obtained for the final product together with the molar ratios Pd/PEG, Co/PEG, K/PEG and CN/PEG in the reaction mixture and in the final material. It is to be observed that n_{Pd}/n_{PEG}, n_{Co}/n_{PEG} and n_{CN}/n_{PEG} are practically the same in the reaction mixture and in the final product, indicating that quite similar molar amounts of Pd, Co and PEG are lost during shrinkage and release of the catalyst water (step c) of Scheme 1). The increase in the n_K/n_{PEG} ratio in the product with respect to the value in the reaction mixture supports the proposed reaction scheme and clearly shows that

TABLE 2: Microanalytical Data (%) and Molar Ratios for Polymeric $[Co_xPd_y(CN)_zCl_v(C_{2n}H_{4n+2}O_{n+1})K_l]$

microanalytical data		molar ratios		
			reagents[a]	product
Pd	3.97	n_{Pd}/n_{PEG}	0.2050	0.2730
Co	0.88	n_{Co}/n_{PEG}	0.1052	0.1098
K	5.38	n_K/n_{PEG}	0.7260	1.0073
N	1.13	n_{CN}/n_{PEG}	0.6321	0.5908
C	44.32			
H	7.90			

[a] Calculated by using the data reported in Table 1 after excluding water.

the direct and indirect nucleophilic substitution of Cl^- in $PdCl_4^{2-}$ takes place, giving rise to a polymer electrolyte doped in situ with KCl.

Rheological Measurements. The sol → gel transition (step b) of Scheme 1) was investigated by rheological measurements using a dynamic oscillatory method.[23] Only small sinusoidal mechanical deformations (0.5 Pa) were applied to the material to avoid any interference with the gelation process below the gel point. This analysis was carried out in the linear viscoelastic region and allowed us to obtain information about the state of the liquid, viscoelastic fluid and gel solid during the sol → gel transition process as a function of time, and to monitor the structural modification of the gel network with time. Moreover, the value of the strain which irreversibly breaks the gel structure above the gel point (the brittle point after gelation at time t) was determined by applying an increasing degree of mechanical deformation to the material at a fixed frequency of 1 Hz.

The rheological results are presented in terms of the "complex shear modulus" G^* through the equation[23]

$$G^* = G' + iG''$$

where G' and G'' are referred to as the "storage" (or elastic) modulus and "loss" (or viscous) modulus, respectively. They correspond to the in-phase and out-of-phase components of the resulting stress and are linked to the real and imaginary components of the complex viscosity η^* by the relations $G' = \omega\eta''$ and $G'' = \omega\eta'$. Another parameter widely used in the characterization of the linear viscoelastic response of materials is the "loss angle" δ, which is defined as $\tan\delta = G''/G' = \eta'/\eta''$.

The logarithms of the rigidity modulus (G') and of the loss modulus (G'') together with δ against frequency measured 35 min and 6 h after mixing of solutions A and B are reported in Figure 1a,b, respectively. This analysis was performed at 40 °C. The behavior depicted in Figure 1a indicates that (a) for $\omega \cong 6.3$ (rad/s), the G' and G'' curves intersect together; (b) for $\omega < 6.3$ (rad/s), G'' is higher than G'; and (c) an opposite order in the dependence on frequency is detected for $\omega > 6.3$ (rad/s). As reported in the literature,[24] this frequency-dependent rheological response is typical of viscoelastic liquids.

After 6 h at 40 °C the dependence of G' and G'' on frequency is substantially changed (Figure 1b). Indeed, the rigidity modulus G' is always higher than G'' and is practically independent of frequency. It should be noted that in a perfect gel the stresses cannot relax and consequenly G' remains constant regardless of frequency and dominates in value.[24]

Figure 1c reports the dependence of G' and G'' on the logarithm of the applied strain to the gel above the gel point. It is to be observed that a sudden decrease in the elastic modulus and an increase in the viscous modulus are observed when we apply a strain of ≅316 Pa. At this strain point (brittle point

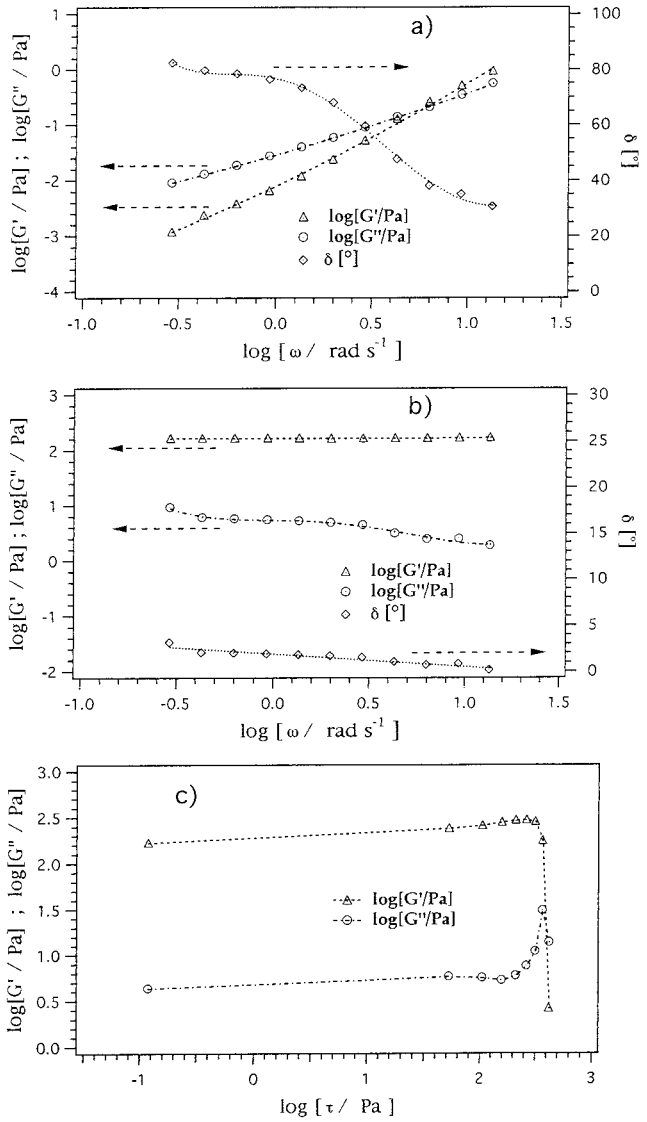

Figure 1. G', G'' and δ (deg) versus frequency plots measured after a reaction time of 35 min (a) or 6 h (b). (c) G', G'' as functions of logarithm of stress (τ/Pa) measured after a reaction time of 6 h. The time when solutions A and B were mixed was taken as $t = 0$ (see experimental section).

after 6 h of reaction time, measured at 40 °C) the gel fractures irreversibly, thus indicating that the gel material is brittle.

Taking into account that, during gel formation, the number of interchain cross-links in a polymeric gel network are proportional to the elastic modulus,[25] the kinetics of the gelation process was studied at different temperatures by monitoring G' and G'' as a function of time. The dependence of G' and G'' versus time at 0.5 Pa of applied strain and at 1 Hz of frequency are reported in Figure 2a,b, respectively. It is to be observed that the storage modulus increases in a sigmoidal fashion as cross-links start to form and reaches a plateau when the network has been completely constructed. It is well-known that the gel point is detected when the last cross-link occurs[25] so that the entire network of macromolecules links together to become space-filling. After this point, G' remains quite constant with time, and the material will break apart if a sufficiently large strain is applied[23] (see Figure 1c). The same behavior is observed for G'' (see Figure 2b). Two steps are observed in the profiles of G' vs time. These functional dependences can easily be explained if we consider that (a) at times prior to that corresponding to the first plateau, direct substitution of the Cl^- in $PdCl_4^{2-}$ by H_2O or nitrogen of cyanometalate ligands is likely to predominate, giving rise to a viscoelastic solution, and (b) after the first plateau, H_2O is displaced by the hydroxyls of PEG600 and nitrogen of cyanometalate ligands, producing a subsequent increase in interchain cross-links which are probably responsible for the viscoelastic solution → hard gel transition, concluded at the gel point.

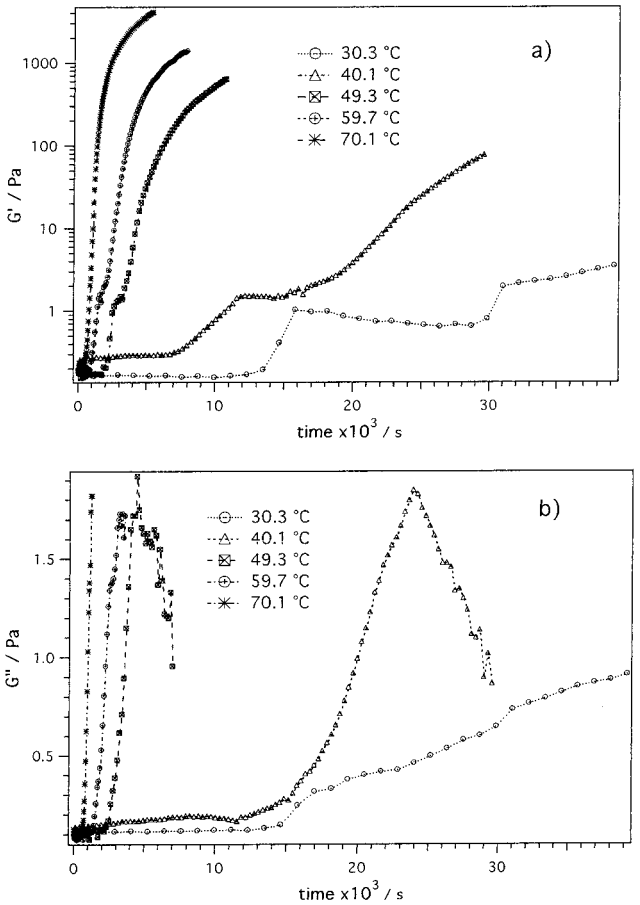

Figure 2. Plots of the elastic G' (a) and viscous modulus G'' (b) versus time for the sol → gel transition at various temperatures. Time measurements were performed as described in Figure 1.

The dependence of the gel point time (gel time) and the logarithm of rigidity modulus at the gel point time ($G'_{\text{gel point}}$) on temperature are shown in Figure 3a,b, respectively. Figure 3a clearly shows that the gel point time (g_p) decreases linearly with temperature (T) ($g_p = 3.086 \times 10^{-5} - 894.74T$; $R = 0.97$) thus indicating that irreversible reactions with very low activation energies occur during the sol → gel transition. This observation indicates that the interchain cross-link rate rises as the reaction temperature increases. Furthermore, $G'_{\text{gel point}}$ increases exponentially with reaction temperature (see Figure 3b), thus indicating that the number density of interchain cross-links in the gel network rises with the reaction temperature. Therefore, we can conclude that the gelation process carried out at higher temperatures produces the most robust solid gel structure at the highest reaction rate possible.

Thermal Analysis, Morphology and Electrochemical Stability. The thermal stability of the final Z-IOPE product was investigated by TG analysis. As demonstrated by the thermogram of the material reported in Figure 4, this polymer is thermally stable up to ca. 210 °C and decomposes at approximately 230 °C. The TG measurements also indicate that the network does not contain detectable amounts of entrapped water. The first mass lost at 230 °C could be attributed to

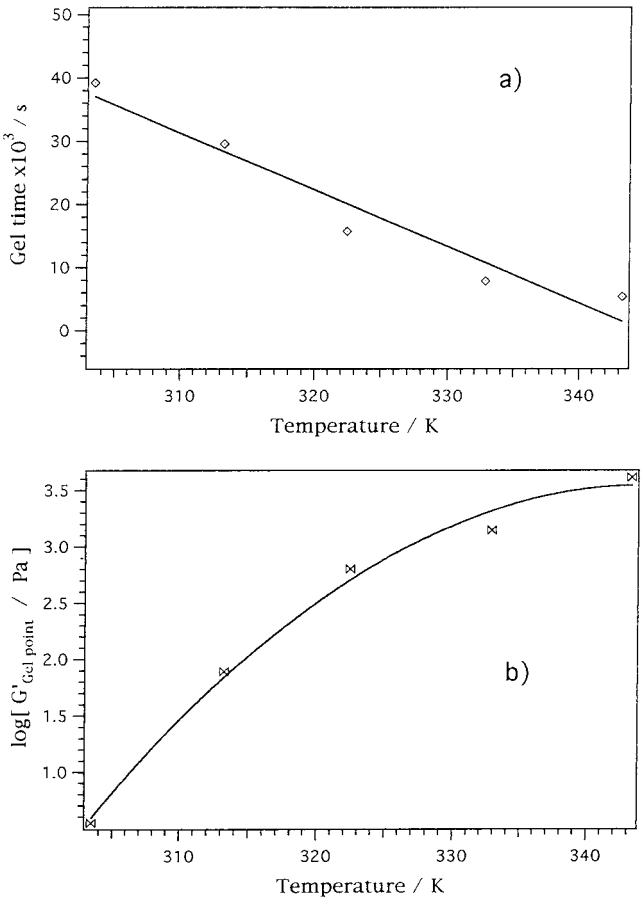

Figure 3. Dependence of the gel time on temperature (a) and plot of the logarithm of the elastic modulus at gel time ($G'_{\text{gel point}}$) as a function of temperature (b). Gel time corresponds to the time at which an inflection in the plot $G' = f(t)$ is registered (i.e., when the sigmoidal portion of the curve ends and starts to plateau).

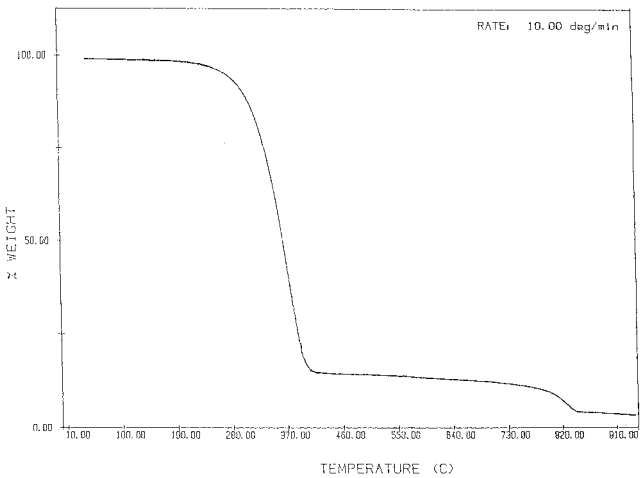

Figure 4. TG measurements of the $[Co_xPd_y(CN)_zCl_v(CH_{2n}H_{4n+2}O_{n+1})\text{-}K_l]$ electrolytic complex.

PEG600 decomposition;[17] the loss of ca. 4.7% of the total weight in the 550−750 °C temperature range could be associated with the elimination of cyanide as cyanogen $(CN)_2$ from the Co metal center;[26,27] and the last loss of mass, detectable in the 750−900 °C range, could be assigned to KCl sublimation.[28]

The morphology of the Z-IOPE was investigated by scanning electron microscopy (SEM). The resulting micrograph shown in Figure 5 demonstrates that this material is constituted by a compact granular paste. Close examination reveals two types of grains having mean diameters of approximately 200 μm and $\cong$50 μm.

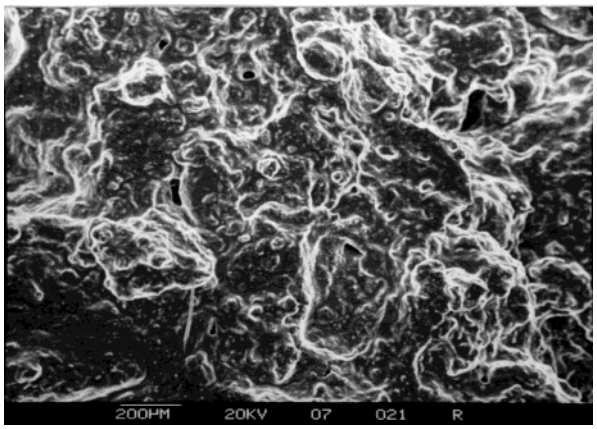

Figure 5. SEM micrograph of the $[Co_xPd_y(CN)_zCl_v(CH_{2n}H_{4n+2}O_{n+1})\text{-}K_l]$ electrolytic complex.

The microanalysis carried out by X-ray fluorescence with energy dispersive spectroscopy (XRD-EDS) showed that O, Cl, Pd, K and Co are uniformely distributed in the bulk material. However, the backscattered image indicated that the Z-IOPE material incorporates microcrystals which, on the basis of XRD-EDS analysis, consist of KCl embedded in the microparticles of the material.

To identify the useful potential window of the polymer electrolyte, its electrochemical stability was investigated by voltametric studies carried out as described in the Experimental methods section. The resulting voltammogram showed that the material is electrochemically stable from 1.250 V to −0.908 V, thus indicating that the useful potential window of this polymer electrolyte is of ca. 2.16 V.

FT-IR Spectroscopy. The FT-IR spectra in the mid-(MIR) and far-infrared (FIR) regions are depicted in Figure 6a,b, respectively.

Figure 6a shows that this material presents two general spectral features in the MIR region, one directly correlated with the PEG moiety of the material and the other associated with the stretching of CN groups (2000−2300 cm^{-1}). In the 3500−3000 cm^{-1} region, two bands peaking at 3482 and 3335 cm^{-1} are detected, which are associated with the ν^a(OH) and ν^s(OH) stretching vibrations of PEG600.[29] The bands in the 800−1000 and 1200−1600 cm^{-1} regions are vibrational modes diagnostic for the conformation of the poly(ethylene glycol) chains.[29,30] The frequency values of these spectral regions coincide with those corresponding to a PEG chain in a $D(4\pi/7)$ factor group, which assumes the TGT conformation[30] (T = trans, G = gauche) where $\tau(CH_2-CH_2) = 60°$ (gauche) and $\tau = (O-CH_2) = \tau(CH_2-O) = 191.5°$ (trans).

As previously reported,[30] the C−O stretching vibrations detected in PEG600 at 1123 (E_1), 1031 (E_1) and 1000 (E_1) cm^{-1} are diagnostic vibrations for the salt-polyether chain complexation process. In the Z-IOPE complex, these vibrations are observed at 1107 (E_1), 1038 (E_1) and 997 (E_1) cm^{-1}, respectively, i.e., at lower frequencies and with a higher intensity with respect to pure PEG600. These observations lead to the proposal that the oxygen atoms in the polyether chains are involved in K^+ coordination. On the other hand, in agreement with the literature,[30] the peak centered at 1069 (A_2) cm^{-1} could be attributed to the terminal C−O vibration of PEG600 chains, which is probably responsible for cross-links in the polymer reaction through the coordination of Pd atoms.

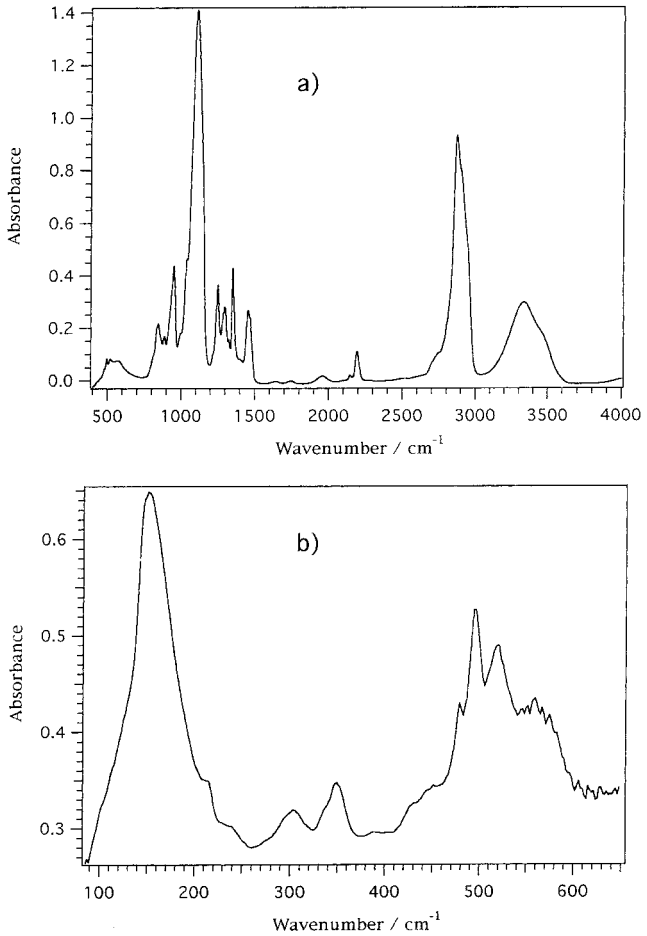

Figure 6. FT-IR absorption spectra of the $[Co_xPd_y(CN)_zCl_v(CH_{2n}H_{4n+2}O_{n+1})K_l]$ electrolytic complex: (a) MID; (b) FIR.

In the MIR region of the CN vibrations, four intensities of bands peaking at 2106, 2148, 2194, and 2227 cm^{-1} are observed.

The absorption at 2106 cm^{-1} is correlatively assigned to the $\nu(-CN)_t$ vibration of the terminal CN groups,[17,31−33] while those at 2148, 2194, and 2227 cm^{-1} are associated with the $\nu(-CN)_b$ modes of the Co−CN−Pd bridging cyanide groups.[17,32,33]

The far-IR spectrum of the Z-IOPE is depicted in Figure 6b. The peak measured at 567 cm^{-1} and the two bands peaking at 447 and 428 cm^{-1} were assigned to δ(Co−CN) bending and ν(Co−C) stretching, respectively.[34] The two peaks at 519 and 496 cm^{-1} are attributed to the ν^a(Pd−N) and ν^s(Pd−N) vibrational modes, respectively.[35] Similarly, the two bands found at 349 and 303 cm^{-1} were correlatively assigned to the ν^a(Pd−Cl) and ν^s(Pd−Cl) vibrations, respectively.[35] It should be noted that the presence of the doublets representing ν(Pd−N) and ν(Pd−Cl) vibrations in the far-IR spectrum is indicative of the fact that Pd atoms are coordinated by nitrogen ligands in a cis configuration.[35,36] The absorptions at 478 and 237 cm^{-1} were attributed to ν(Pd−O) stretching vibrations.[37] These results confirm that the Z-IOPE material is formed owing to the substitution of chloride ligands in $[PdCl_4^{2-}]$ by nitrogen and oxygen atoms supplied by the CN and PEG600 hydroxyl groups, respectively.

The complete assigments of the MIR and far-IR FT-IR spectra are summarized in Table 3. These results suggest the following structural features: (a) CN bridges may be present between Co and Pd atoms, (b) PEG600 bridges may link Pd atoms together, and (c) the conformation of PEG600 chain in the material is of the TGT type.

Semiquantitative information regarding the concentration of bridging and terminal cyanide groups in the Z-IOPE system was obtained by Gaussian spectral decomposition of the spectrum in the 1850−2400 cm^{-1} region. This analysis, which was performed after background corrections and normalization of the spectrum,[38] permitted us to determine the number of spectral components, the peak positions, and the shape of each ν(CN) vibrational mode (Figure 7). The peak positions, the full width at half-height (fwhh) and the band areas are reported in Table 4. The percentage of each type of structurally different CN with respect to the total amount of CN groups was obtained by calculating R_i (%) = $A_i100/\sum$, where A_i is the band area contributed by a defined type of CN group and $\sum = \sum_{i=1}^{4} A_i$.

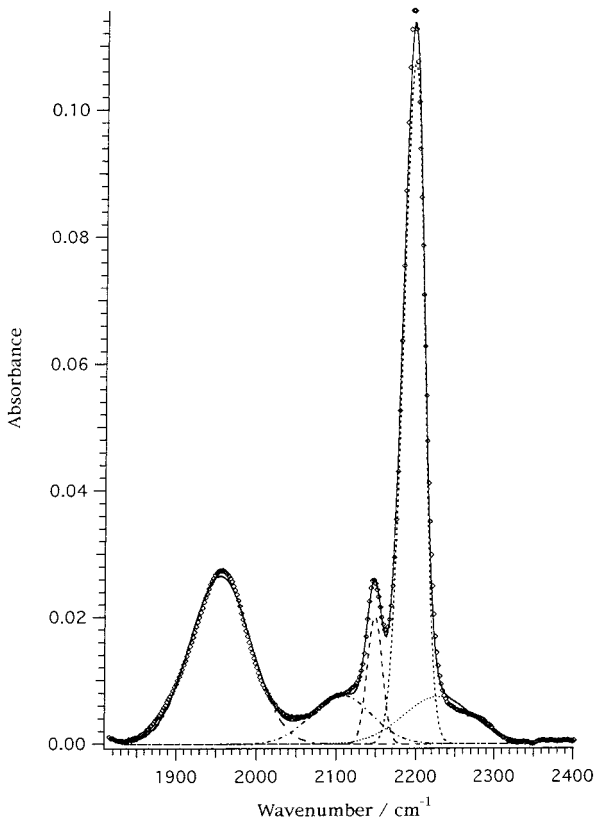

Figure 7. Decomposition by Gaussian functions of the MID FT-IR spectral range from 1850 to 2350 cm^{-1} of the $[Co_xPd_y(CN)_zCl_v(CH_{2n}H_{4n+2}O_{n+1})K_l]$ electrolytic system.

Similarly, by using the data reported in Table 4, it was possible to determine the fractional amount of the CN bridging (R^{CN_b}) and terminal (R^{CN_t}) groups ($R^{CN_b} = (A_{2227} + A_{2194} + A_{2148})/\sum$) and $R^{CN_t} = A_{2106}/\sum$). The values of R^{CN_b} and R^{CN_t} were 0.85 and 0.13, respectively (see Table 4), indicating that, among the 6 CN groups in the Z-IOPE material, one is probably of the terminal type ($\cong$1/6) and the remaining five are bridging cyanides ($\cong$5/6). On the basis of the analytical data reported in Table 2, it is possible to determine the following ratios: $f_M = (n^{Co} + n^{Pd})/N = 0.277 \cong 0.3 \equiv 3/10$; $f_{PEG} = n^{PEG}/N = 0.723 \cong 0.7 \equiv 7/10$; $f^{Co} = (n^{Co}/N_M = 0.29 \cong 0.3 \equiv 1/3$ and $f_{Pd} = n^{Pd}/N_M = 0.71 \cong 0.7 \equiv 2/3$; where $N = n^{Co} + n^{Pd} + n^{PEG}$, $N_M = n^{Co} + n^{Pd}$ and n^{Co}, n^{Pd} and n^{PEG} are the moles of Co, Pd and PEG600, respectively, in 100 g of Z-IOPE material.

The values for f_M and f_{PEG} indicate that each 10 moles of components in Z-IOPE are composed of three moles of metals (Co + Pd) and seven of PEG600; f_{Co} and f_{Pd} specify that of the three moles of metals, one is Co and two are Pd atoms.

Taking into consideration these calculations and results of the far-IR analysis, which demonstrated the presence of Pd−

TABLE 3: Molecular Vibration Assignments of the $[Co_xPd_y(CN)_zCl_v(C_{2n}H_{4n+2}O_{n+1})K_i]$ Polymer[a]

species	wavenumber in cm^{-1} obsd[b]	wavenumber in cm^{-1} calcd[c]	assignment and potential-energy distribution[c,d]	ref
A_2	3482 (m)		ν^a(OH)	29, 30
	3335		ν^s(OH)	29, 30
	2876 (s)	2883	$\nu^s(CH_2)$ (100)	30
	2227 (vw) 2194 (w) 2148 (vw)		$\nu(-CN)_b$	17, 32, 33
	2106 (vw)		$\nu(-CN)_t$	17, 31, 32, 33
	1470 (m) 1456 (m)	1470	$sr(CH_2)$ (100)	30
	1350 (m) 1325 (vw)	1344	$w(CH_2)$ (107)	30
	1250 (m)	1264	$t(CH_2)$ (81)	30
	1069 (vs sh)	1087	ν(CO) (94)	30
	953 (m)	964	$r(CH_2)$ (49), $t(CH_2)$ (18)	30
	567 (w)		δ(Co−CN)	34
	559	533	δ(CCO) (89), $r(CH_2)$ (33)	30
	519 (s)		ν^a(Pd−N)	35
	496 (vs)		ν^s(Pd−N)	35
	478 (w)		ν(Pd−O)	37
	447 (w) 428 (w)		ν(Co−C)	34
	390 (w)			
	349 (m)		ν^a(Pd−Cl)	35
	303 (m)		ν^s(Pd−Cl)	35
	237 (vw)		ν(Pd−O)	37
	150 (vs)		ν(Pd−Cl)	36
E_1	2936 (sh)	2940	$\nu^a(CH_2)$, (101, 18°)	30
	2845 (vs)	2873	$\nu^s(CH_2)$, (100, −5)	30
	1487 (w)	1471	$sr(CH_2)$, (100, −132°)	30
	1439 (sh)	1401	$w(CH_2)$, (95, 53°)	30
	1360 (sh)	1353	$w(CH_2)$, (107, −129°)	30
	1294 (m)	1286	$t(CH_2)$, (73, −40°)	30
	1223 (w)	1234	$t(CH_2)$, (87, 116°)	30
	1148 (vw)	1142	ν(CO), (37, −27°), $r(CH_2)$, (29, −66°)	30
	1107 (vs)	1112	ν(CO), (81, 136°), ν(C−C) (21)	30
	1038 (w)	1060	ν(CO), (36, −102°) $r(CH_2)$, (35, 70°), ν(CC) (17)	30
	997 (vw)	941	$r(CH_2)$, (34, 42°), ν(CC) (27), ν(CO) (14, 167°)	30
	887 (w) 845 (w) 833 (w)	847	$r(CH_2)$, (58, −149°), ν(CO), (39, −9)	30 30
	525 (vw)	524	δ(COO), (43, −142°), δ(COC), (21), $r(CH_2)$ (17, 152°)	30
	300 (w)	366	δ(CCO), (42, −73°), δ(COC) (38)	30
	160 (w)	164	ϕ_i(CC) (42), ϕ_i(CO) (38, −161°), δ(CCO) (18, 16°)	30

[a] PEG600 was assumed under the $D(4\pi/7)$ symmetry group. [b] Relative intensities are reported in parentheses. Key: vs, very strong; s, strong; m, medium; w, weak; vw, very weak; sh, shoulder. [c] The normal coordinate analysis was derived from the references reported in the last column. [d] Key: ν, stretching; δ, bending; w, wagging; t, twisting; r, rocking; sr, scissoring; ϕ_i, internal rotation; a, antisymmetric mode; s, symmetric mode.

TABLE 4: Band Parameters of the ν(CN) FT-IR Vibrational Modes for Polymeric $[Co_xPd_y(CN)_zCl_v(C_{2n}H_{4n+2}O_{n+1})K_i]$[a]

	v/cm^{-1}	A	FWHH	R_i (%)	R^{CN_i}	R^{CN}_{teo}
$\nu(-CN)_b$	2227	0.8175	102.8	14.73	$R^{CN_b} = 0.86$	≈5/6
	2194	3.5294	30.8	63.62		
	2148	0.4737	22.1	8.54		
$\nu(-CN)_t$	2106	0.7267	88.7	13.10	$R^{CN_t} = 0.13$	≈1/6

[a] A, band area; fwhh, full width at half-height; R_i (%) = $A_i 100/\sum_{i=1}^{4} A_j$; $R^{CN_b} = (A_{2227} + A_{2194} + A_{2148})/\sum_{i=1}^{4} A_i$; $R^{CN_t} = A_{2106}/\sum_{i=1}^{4} A_i$.

O, Pd−Cl, Co−C and Pd−N bonds, we propose that the Z-IOPE assumes the structure depicted in Scheme 2.

Impedance Studies. The conductivity of the inorganic−organic polymer electrolyte was analyzed by impedance spectroscopy (IS) carried out at different temperatures. The resulting Nyquist plots are characterized by a single semicircle (typical for a geometrical capacitance and a bulk resistance in parallel with it) and by spikes at low frequencies associated with diffusion-limited Warburg impedancies.[39]

SCHEME 2: Structure Proposed for the $[Co_xPd_y(CN)_zCl_v(CH_{2n}H_{4n+2}O_{n+1})K_i]$ Network

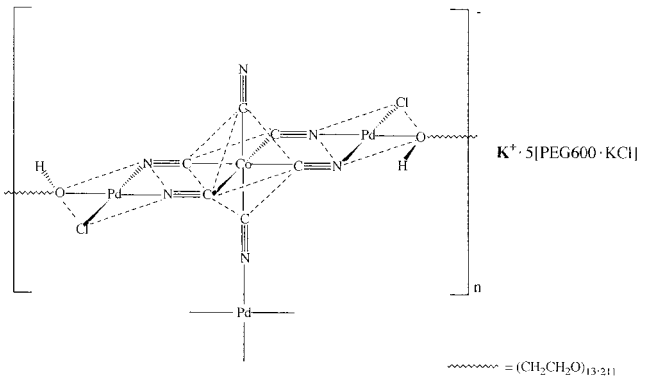

The impedance data were fitted by assuming an equivalent circuit composed of a parallel circuit in series with a constant phase element (CPE_w); the parallel circuit was constituted by a constant phase element (CPE − 1_b) in parallel with an

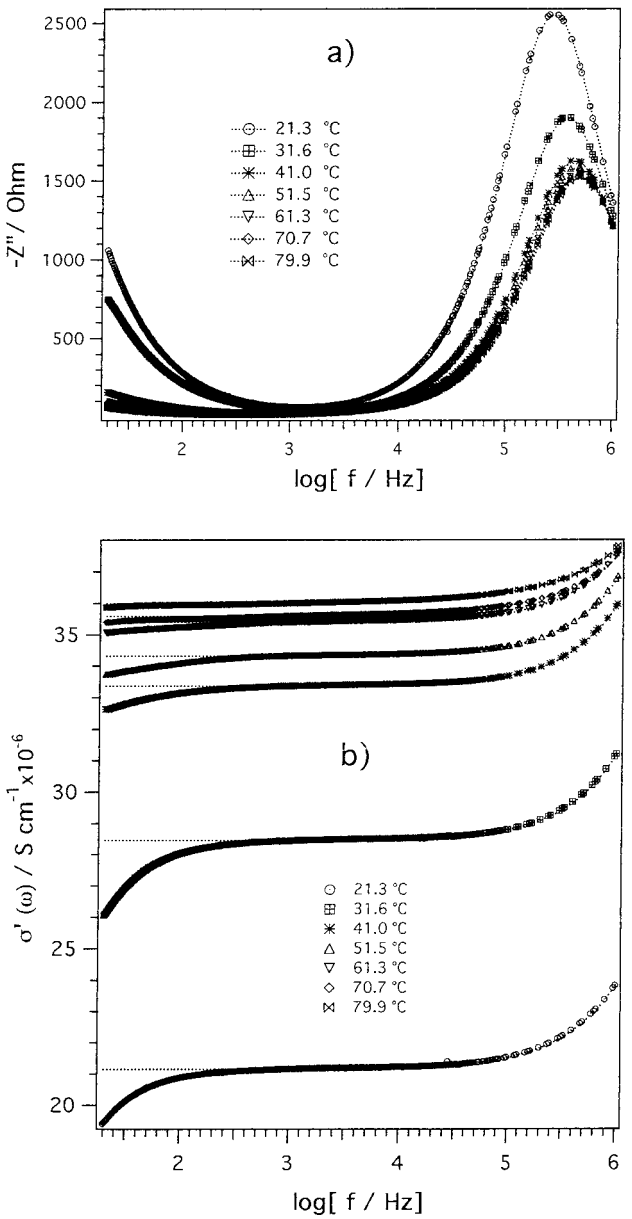

Figure 8. Imaginary (Z'') component of the complex impedance versus log f (Hz) for the $[Co_xPd_y(CN)_zCl_v(CH_{2n}H_{4n+2}O_{n+1})K_l]$ electrolytic polymer (a). $\sigma'(\omega)$ versus log f (Hz) at various temperatures (b). Dotted lines show the curves obtained by fitting $\sigma'(\omega) = \sigma(0)[1 + (\tau_1\omega)^p]$ to $\sigma'(\omega)$ using experimental data at frequencies higher than 0.4 kHz. The data were fit using nonlinear least-squares procedures.

impedance (Z_b). It should be noted that although several other equivalent circuits were tested, the data fit this one most satisfactorily. The fittings were carried out by using the EQUIVCRT program written by Boukamp.[40] The constant phase element (CPE $-$ 1_b) in parallel with the impedance (Z_b) always exhibited a n_c value close to unity, thus indicating that this element corresponds to a capacitance (C). Furthermore, the CPE_w element, in series with the parallel circuit, always yielded $n_w \cong 0.5$, suggesting a Warburg dispersion.[29,39] The bulk resistances determined by this fitting procedure allowed us to obtain the conductivities of the Z-IOPE material.

A plot of the imaginary component of impedance, Z'', vs the decimal logarithm of the frequency in Figure 8a revealed a typical Debay peak[41] centered in the $5 \leq \log[f/\text{Hz}] \leq 6$ range.

By using the R and C parameters obtained by equivalent circuit fitting of the RC parallel, we can calculate $\sigma'(\omega) = 1/kR$, where k is the cell constant in cm and R is the resistance, which

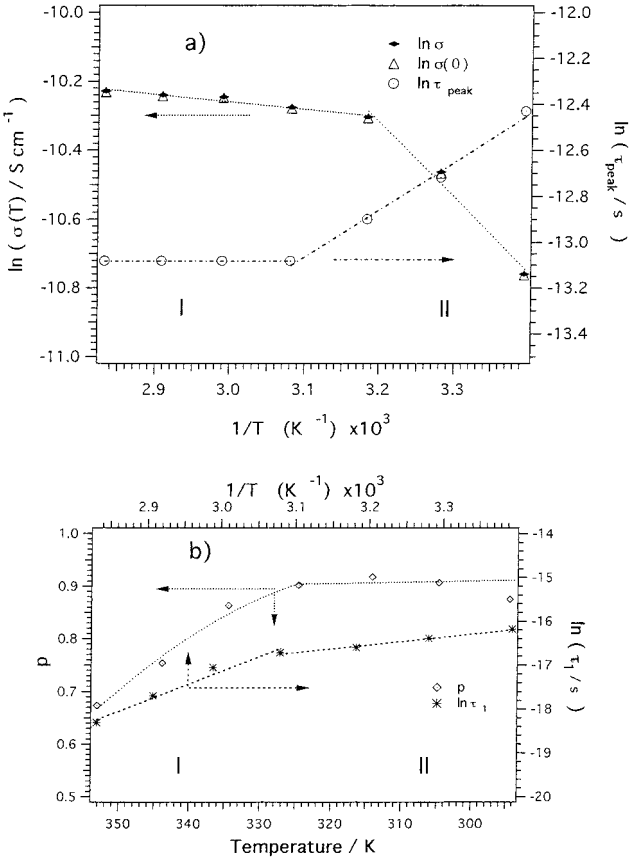

Figure 9. Dependence of ln σ, ln $\sigma(0)$ and ln τ_{peak} on temperature (a). Plots of p and ln τ_1 as a function of temperature (b). Conductivity regions I and II are indicated.

is independent of frequency. $\sigma'(\omega)$ calculated from impedance data by the equation $\sigma'(\omega) = Z'(\omega)/[(Z'(\omega))^2 + (Z''(\omega))^2]k$ exhibits the frequency dependence shown in Figure 8b. These curves consist of the following three distinct regions: (a) a low-frequency spike, (b) a medium-frequency plateau and (c) a high-frequency spike. The high-frequency portion of the curves cannot be justified by the simple equivalent circuit analysis and is assigned to the correlated ionic motions in the material.[42,43]

The medium plateau region is associated with $\sigma_{DC} = \sigma'(\omega) = 1/kR$ of the bulk material and the low-frequency spikes describe the Warburg dispersion phenomenon. Both these latter phenomena are well rationalized by the equivalent circuit analysis.[44]

Therefore, full characterization of the AC electrical response of the Z-IOPE material requires both equivalent circuit analysis and correlated ionic motion analysis, which is based on the jump relaxation model.[42,43,45] This latter investigation was carried out by fitting to the data shown in Figure 8b the Universal Power Law (UPL) equation:[45]

$$\sigma'(\omega) = \sigma(o)[1 + (\omega\tau_1)^p] \qquad (1)$$

where $\sigma(o) = \sigma_{DC}$, τ_1 is a time correlated with the initial site relaxation time of ion hopping τ_2, $p = \tau_2/\tau^*$ is the power-law exponent and τ^* is the initial back-hop relaxation time.

Equation 1 fits very well with experimental data in the medium and high-frequency regions (Figure 8b) using a nonlinear least-squares fitting procedure. The fitted curves are represented by dotted lines in Figure 8b.

Figure 9 shows plots of all the parameters obtained by the equivalent circuit and UPL analyses plotted versus temperature.

TABLE 5: Parameters Determined by Fitting Arrhenius Type Equations to the Dependence of $\sigma(T)^a$, $\tau_{peak}(T)^b$ and $\tau_1(T)^c$ Data against Temperature (see Figure 10)

region	A_σ (S·cm^{-1})	τ^o_{peak} (s)	τ^o_1 (s)	E_a (kJ·mol^{-1})	E_{peak} (kJ·mol^{-1})	E_{s-r} (kJ·mol^{-1})
I	$6.71 \times 10^{-5} \pm 1 \times 10^{-7}$	2.082×10^{-6}	$1.175 \times 10^{-16} \pm 3 \times 10^{-17}$	$1.7996 \pm 4 \times 10^{-4}$	-	54.163 ± 0.03
II	$3.20 \times 10^{-2} \pm 6 \times 10^{-3}$	$3.685 \times 10^{-9} \pm 7 \times 10^{-11}$	$2.44 \times 10^{-10} \pm 5 \times 10^{-12}$	17.87 ± 0.07	17.057 ± 0.003	$14.553 \pm 3 \times 10^{-3}$

^{a} $\sigma(T) = A_\sigma e^{-E_a/RT}$. ^{b} $\tau_{peak}(T) = \tau^o_{peak} e^{+E_{peak}/RT}$. ^{c} $\tau_1(T) = \tau^o_1 e^{+E_{a-r}/RT}$.

As expected, the values for σ obtained from the equivalent circuit analysis coincide exactly with those obtained by eq 1, and clearly show that two conductivity regions are to be distinguished depending on the temperature of the material (Figure 9a). The conductivity regions I and II, which are located in the 40−80 and 40−20 °C temperature regions, respectively, are well described by Arrhenius type equations:

$$\sigma(T) = A_\sigma e^{-E_a/RT} \quad (2)$$

where A_σ is a preexponential factor and E_a is the activation energy for conduction.

In Table 5 are summarized the parameters determined by fitting eq 2 to the data reported in Figure 9a.

The imaginary component of the impedance (Figure 8a) shows a dielectric relaxation time $\tau_{peak} = 1/f_{peak}$ (s), where f_{peak} is the frequency in Hz at the maximum of the Debye peak.[41] τ_{peak} is independent of temperature in region I while in region II it exhibits an Arrhenius type behavior ($\tau_{peak} = \tau^0_{peak} e^{+E_{peak}/RT}$), as shown in Figure 9a. Table 5 also reports the parameters determined by fitting the Arrhenius type equation to τ_{peak} data as a function of temperature. These results indicate that (a) A_σ, which is proportional to the charge carrier concentration in the Z-IOPE material, is higher in region II than in region I, (b) the activation energy for conduction (E_a) is very low in region I, whereas that obtained by τ_{peak} (E_{peak}) is zero, and (c) in region II, $E_a \cong E_{peak} \cong 17$ kJ mol^{-1}. All these observations provide a strong indication that the investigations carried out using the conductivity and Debay peak relaxation times are equivalent. Indeed, both these approaches are correlated to the overall conduction mechanism of the material.

Further information on the ion dynamics in the Z-IOPE system is obtained by considering the temperature dependence of the parameters obtained by fitting eq 1 to the data of Figure 8b. Figure 9b shows the dependence of the power law exponent[45,42] p on temperature.

It is well-known that p = (initial back-hop rate)/(initial site relaxation rate); conductivity occurs "successfully" when the "initial site relaxation rate" $= 1/\tau_2 = r_s$ in the host material is higher than the "initial back-hop rate" $= 1/\tau^* = r_b$ of the ions.[42,43,45]

It can be observed that $r_s > r_b$ at all of the temperatures tested. Particularly, in region I, as temperature increases, p decreases from ≅0.9 to ≅0.6, whereas in region II, p always assumes a constant value of ≅0.9. These findings demonstrate that at lower temperatures the rate of site relaxation in the host material is slower than at high temperatures. Indeed, in region I site relaxation is gradually favored as the temperature increases. The temperature dependence of τ_1 confirms these results. In both regions I and II, τ_1 depends on temperature and assumes an Arrhenius type behavior, i.e., $\tau_1 = \tau^0_1 e^{+E_{s-r}/RT}$, where E_{s-r} is the site relaxation energy height barrier.[45] The parameters of this Arrhenius type equation for regions I and II are summarized in Table 5. E_{s-r} is highest and p is lowest in region I, leading to the conclusion that ion hopping conductivity in this region is favored while back hopping is inhibited. On the other hand, in region II E_{s-r} is close to E_{peak} and E_a, and p is ca. 0.9, indicating that ion back hopping is responsible for the decrease in conductivity in this region.

These findings lead us to propose that the segmental motion[1,46−48] which in general characterizes the conductivity of polymer electrolyte systems is not detected in the Z-IOPE material. Given that the conductivity of a sample prepared without PEO is of ca. 8.83×10^{-11} S cm^{-1} at 22.0 °C, it is straightforward to conclude that PEO chains are largely responsible for the conductivity of the Z-IOPE. Taken together, these considerations lead us to propose that the polyethereal oxygen atoms, which in TGT PEG chains are directed toward the helix axis, form metal coordination sites[8] that are responsible for the conductivity of this material by an ion hopping mechanism. Our analyses show that this conductivity mechanism involves two distinct phenomena that are well described by the jump relaxation model.[45] The first phenomenon is associated with ion hopping between the sites present in the material along the polyethereal chain (*intrachain hopping*) and between different chains (*interchain hopping*) and the second is associated with the structural relaxation of the host coordination site, which occurs after the ion hopping event. This last phenomenon contributes to the "successful" conductivity of each ion that hops between empty sites.[42] The ion involved in this hopping process is probably K^+, as it is highly unlikely that other cationic species with high molecular weights could be involved in hopping events between empty coordination sites.

Finally, it is to be highlighted that the Z-IOPE material presents a conductivity of ca. 3×10^{-5} S cm^{-1} at 25 °C, thus allowing us to classify it as a good polymer electrolyte.

Conclusions

This paper reports the synthesis of $[Co_xPd_y(CN)_zCl_t(CH_{2n}H_{4n+2}O_{n+1})K_l]$, a new zeolitic polymer electrolyte material based on poly(ethylene glycol) 600, K_2PdCl_4 and $K_3Co(CN)_6$.

Rheological investigations demonstated that this polymer is formed in two steps. At first, a sol → gel transition occurs; this step is favored at increasing temperatures, yielding a harder solid gel. A gel → plastic transition is subsequently observed, which is characterized by a reduction in gel volume and release of the solvent. On the basis of the analytical data and FT-IR studies it was possible to conclude that this material is a mixed inorganic−organic network in which Co and Pd atoms are bonded together by CN bridges and Pd atoms are linked by PEG600 bridges. Furthermore, the complete assignments of the FT-IR spectrum in the far-IR and MIR regions reveal that the PEG600 chains assume a TGT conformation.

This Z-IOPE material is thermally stable up to ≅200 °C and presents the typical granular morphology exhibited by analogous materials prepared by using K_2PdCl_4 and $K_3Fe(CN)_6$.

Conductivity measurements obtained by impedance spectroscopy in the 20−80 °C temperature range and in the 20 Hz to 1 MHz frequency range permitted us to conclude that the Z-IOPE material conducts ionically, most probably through migration of K^+ and Cl^- ions. Two different conductivity regions were detected in the 20 to 80 °C temperature range. Finally, analysis of the conductivity data on the basis of the jump relaxation

model[42,45] suggests that the material conducts via a migration mechanism which involves hopping of ions between bonding sites followed by structural relaxation of the coordination sites.

The conductivity of this electrolytic system at room temperature seems to be quite good ($\cong 3 \times 10^{-5}$ S cm^{-1}); considering that it is very stable and easy to prepare, this new Z-IOPE appears to promise as a profitable material for the development of a new class of electric energy storage systems.

Acknowledgment. Dr. Mirella Zancato and Dr. Michele Marcazzan of Department of Pharmaceutical Sciences are acknowledged for the assistance with rheological measurements.

References and Notes

(1) Gray, F. M. *Polymer Electrolytes, RSC Materials Monographs*; Royal Society of Chemistry: Cambridge, U.K., 1997.
(2) Owen, J. *Chem. Soc. Rev.* **1997**, *26*, 259.
(3) Scrosati, B.; Neat, R. J. In *Applications of Electroactive Polymers*; Scrosati, B., Ed.; Chapman and Hall: London, 1993; p 182.
(4) Wright, P. V. *Elecrochim. Acta* **1998**, *43*, 1137.
(5) Armand, M. *Adv. Mater.* **1990**, *2*, 278.
(6) Vaia, R. A.; Vasudevan, S.; Krawiec, W.; Scaulon, L. G.; Giannelis, E. P. *Adv. Mater.* **1995**, *7*, 155.
(7) Bruce, P. G.; Vincent, C. A. *J. Chem. Soc., Faraday Trans.* **1993**, *89*, 3187.
(8) Di Noto, V.; Bettinelli, M.; Furlani, M.; Lavina, S.; Vidali, M. *Macromol. Chem. Phys.* **1996**, *197*, 375.
(9) Kono, M.; Hayashi, E.; Watanabe, M. *J. Electrochem. Soc.* **1999**, *146*, 1626.
(10) Sun, H. Y.; Sohn, H. J.; Yamamoto, O.; Takeda, Y.; Imanishi, N. *J. Electrochem. Soc.* **1999**, *146*, 1672.
(11) Popall, M.; Andrei, M.; Kappel, J.; Kron, J.; Olma, K.; Olsowski, B. *Electrochim. Acta* **1998**, *43*, 1155.
(12) Skaarup, S.; West, K.; Zachau-Christiansen, B.; Popall, M.; Kappel, J.; Kron, J.; Eichinger, G.; Semrau, G. *Electrochim. Acta* **1998**, *43*, 1589.
(13) Croce, F.; Appetecchi, G. B.; Persi, L.; Scrosati, B. *Nature* **1998**, *394*, 456.
(14) MacFarlane, D. R.; Newman, P. J.; Nairn, K. M.; Forsyth, M. *Electrochim. Acta* **1998**, *43*, 1333.
(15) Di Noto, V.; Furlani, M.; Lavina, S. *Polym. Adv. Technol.* **1996**, *7*, 759.
(16) Münchow, V.; Di Noto, V.; Tondello, E. *Electrochim. Acta* **2000**, *45*, 1211.
(17) Di Noto, V. *J. Mater. Res.* **1997**, *12*, 3393.
(18) Di Noto, V.; Saccon, M.; Bresadola, S.; Zannetti, R. *Analyst (London)* **1990**, *115*, 1041.
(19) Basolo, F.; Pearson, R. G. *Mechanisms of Inorganic Reactions*, 2nd ed.; J. Wiley and Sons: New York, 1967; p 351.
(20) Cotton, F. A.; Wilkinson, G. *Advanced Inorganic Chemistry*, 5nd ed.; J. Wiley and Sons: New York, 1988; p 919.
(21) Rund, J. V. *Inorg. Chem.* **1970**, *9*, 1211.
(22) Rund, J. V. *Inorg. Chem.* **1974**, *13*, 738.
(23) Barnes, H. A.; Hutton, J. F.; Walters, K. In *An Introduction to Rheology*; Rheology Series 3; Elsevier Science Publishers, B. V.: Amsterdam, The Netherlands, 1989; p 46.
(24) Moules, C. A. In *Theoretical and Applied Rheology*; Moldenaers, P., Keunings, R., Eds.; Elsevier Science Publishers, B. V.: Brussels, Belgium, 1992; p 995.
(25) Pfennig, B. W.; Bocarsly, A. B.; Prud'homme, R. K. *J. Am. Chem. Soc.* **1993**, *115*, 2661.
(26) Gallagher, P. K.; Luonro, J. P. *Thermochim. Acta* **1975**, *12*, 159.
(27) Chamberlain, M. M.; Greene, A. F. J. *Inorg. Nucl. Chem.* **1963**, *25*, 1471.
(28) Wendlandt, W. W. *Thermal Analysis*, 3rd ed.; John Wiley and Sons: New York, 1986; p 166.
(29) Di Noto, V.; Lavina, S.; Longo, D.; Vidali, M. *Electrochim. Acta* **1998**, *43*, 1225.
(30) Di Noto, V.; Longo, D.; Münchow, V. *J. Phys. Chem. B* **1999**, *103*, 2636.
(31) Dows, D. A.; Haim, A.; Wilmarth, W. H. *J. Inorg. Nucl. Chem.* **1961**, *21*, 33.
(32) Nakamoto, K. *Infrared and Raman Spectra of Inorganic and Coordination Compounds*, 4th ed.; John Wiley and Sons: New York, 1986; p 272.
(33) El-Sayed, M. F. A.; Sheline, R. K. *J. Inorg. Nucl. Chem.* **1958**, *6*, 187.
(34) Jones, L. H. *J. Chem. Phys.* **1962**, *36*, 1209.
(35) Durig, J. R.; Layton, R.; Sink, D. W.; Mitchell, B. R. *Spectrochim. Acta* **1965**, *21*, 1367.
(36) Hiraishi, J.; Shimanouchi, T. *Spectrochim. Acta* **1966**, *22*, 1483.
(37) Mikami, M.; Nakagawa, I.; Shimanouchi, T. *Spectrochim. Acta* **1967**, *23A*, 1037.
(38) Di Noto, V.; Angelini, E.; Beltramini, M.; Dalla Via, L.; Salvato, B. *Vibr. Spectrosc.* **1998**, *18*, 1.
(39) Macdonald, J. R.; Johnson, W. B. In *Impedance Specroscopy*; Macdonald, J. R., Ed.; John Wiley and Sons: New York, 1987; p 14.
(40) Boukamp, B. A. *Equivalent Circuit (EQUIVCRT. PAS)*; Department of Chemical Technology, University of Twente, PO Box 217, 7500 AE Enschede, The Netherlands, 1989.
(41) Raistrick, I. D.; Macdonald, J. R.; Franceschetti, D. R. In *Impedance Specroscopy*; Macdonald, J. R., Ed.; John Wiley and Sons: New York, 1987; p 48.
(42) Funke, K. *Ber. Bunsen-Ges. Phys. Chem.* **1991**, *95*, 955.
(43) Funke, K. *Z. Phys. Chem.* **1995**, *188*, 243.
(44) Furukawa, T.; Imura, M.; Yuruzume, H. *Jpn. J. Appl. Phys.* **1997**, *36*, 1119.
(45) Cramer, C.; Funke, K.; Saatkamp, T.; Wilmer, D.; Ingram, M. D. *Z. Naturforsch.* **1995**, *50a*, 613.
(46) Ratner, M.; Shriver, D. F. *Chem. Rev.* **1988**, *88*, 109.
(47) Ratner, M. In *Polymer Electrolyte Reviews-1*; McCallum, J. R., Vincent, C. A., Eds.; Elsevier Applied Science: New York, 1989; Chapter 7.
(48) Ratner, M.; Nitzan, A. *Faraday Discuss. Chem. Soc.* **1989**, *88*, 19.